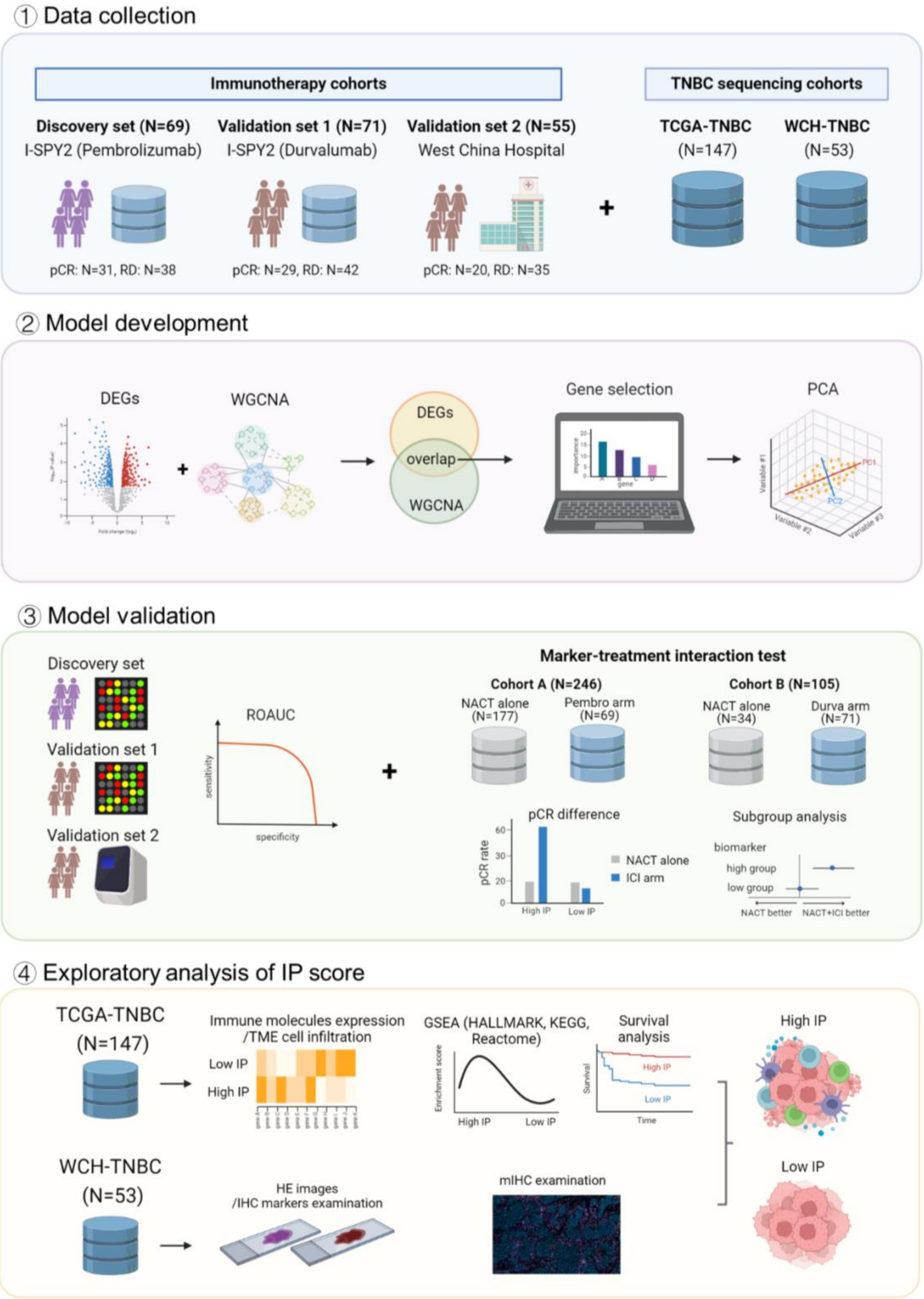

Figure S1. The overall experimental design of this study.

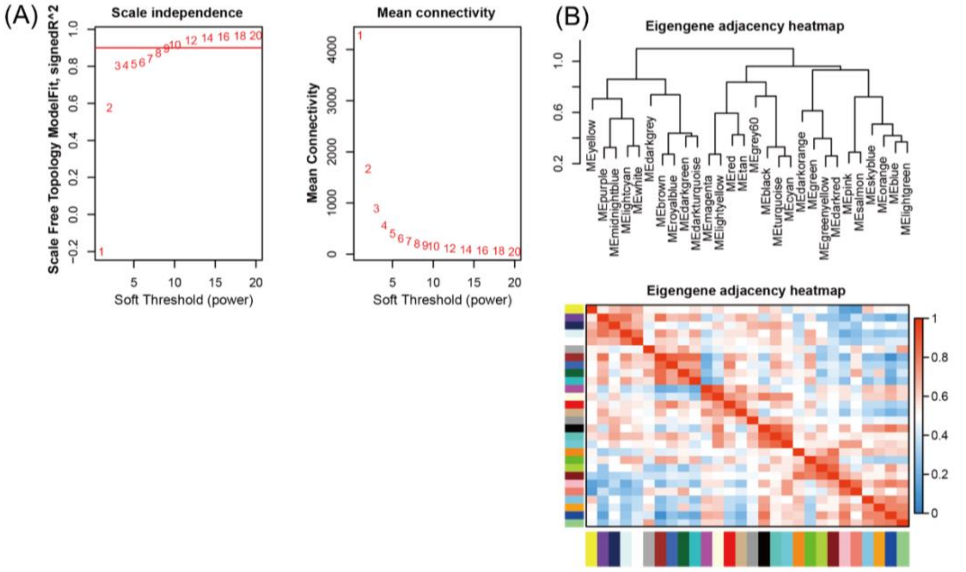

Figure S2. WGCNA analysis for identifying the gene modules related to pCR.

(A) Network topology for different soft-threshold power. The left and right panels show the impact of soft-threshold power on the scale-free topology fit index and the mean connectivity, respectively.

(B) Heatmap indicating the eigengene adjacency of modules.

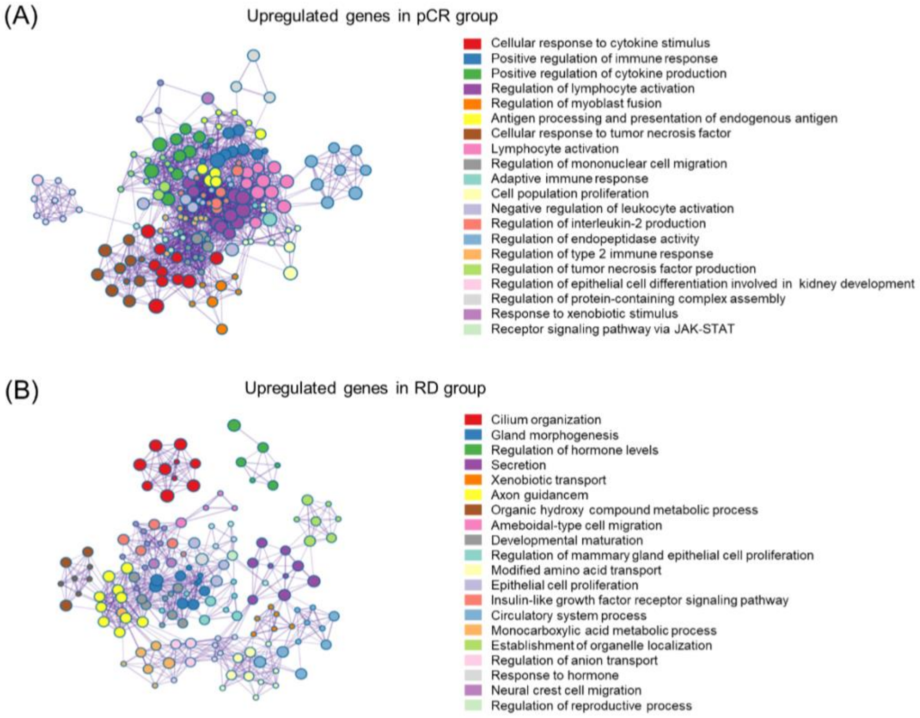

Figure S3. GO function enrichment analysis of candidate genes.

Visualization of enriched GO BP terms of upregulated candidate genes in pCR group (A) and RD group (B) using the Metascape enrichment network.

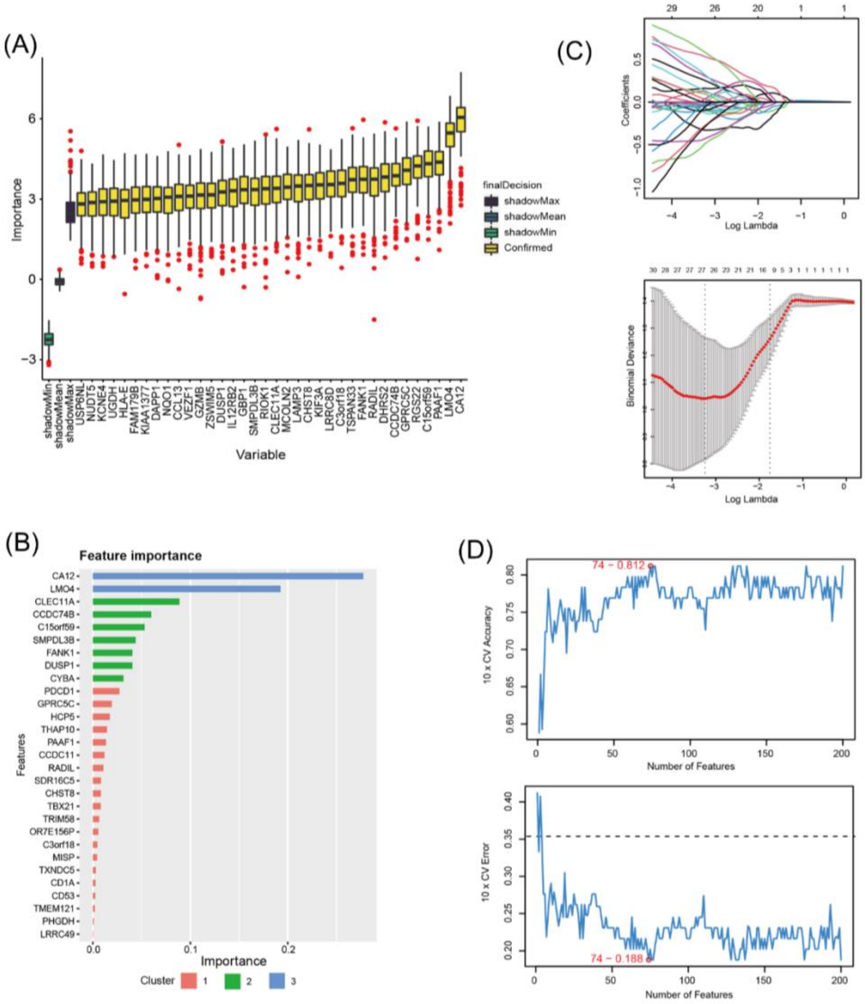

Figure S4. Key gene selection via four machine-learning algorithms.

(A) Importance values of 29 confirmed genes identified by the Boruta algorithm.

(B) Feature importances of genes selected by the XGBoost.

(C) LASSO coefficient profiles of the 405 candidate genes (up) and partial likelihood deviance ± standard error of each lambda (down).

(D) SVM-RFE results show that 74 genes in the model achieve the greatest accuracy (0.812) and the smallest error (0.188).

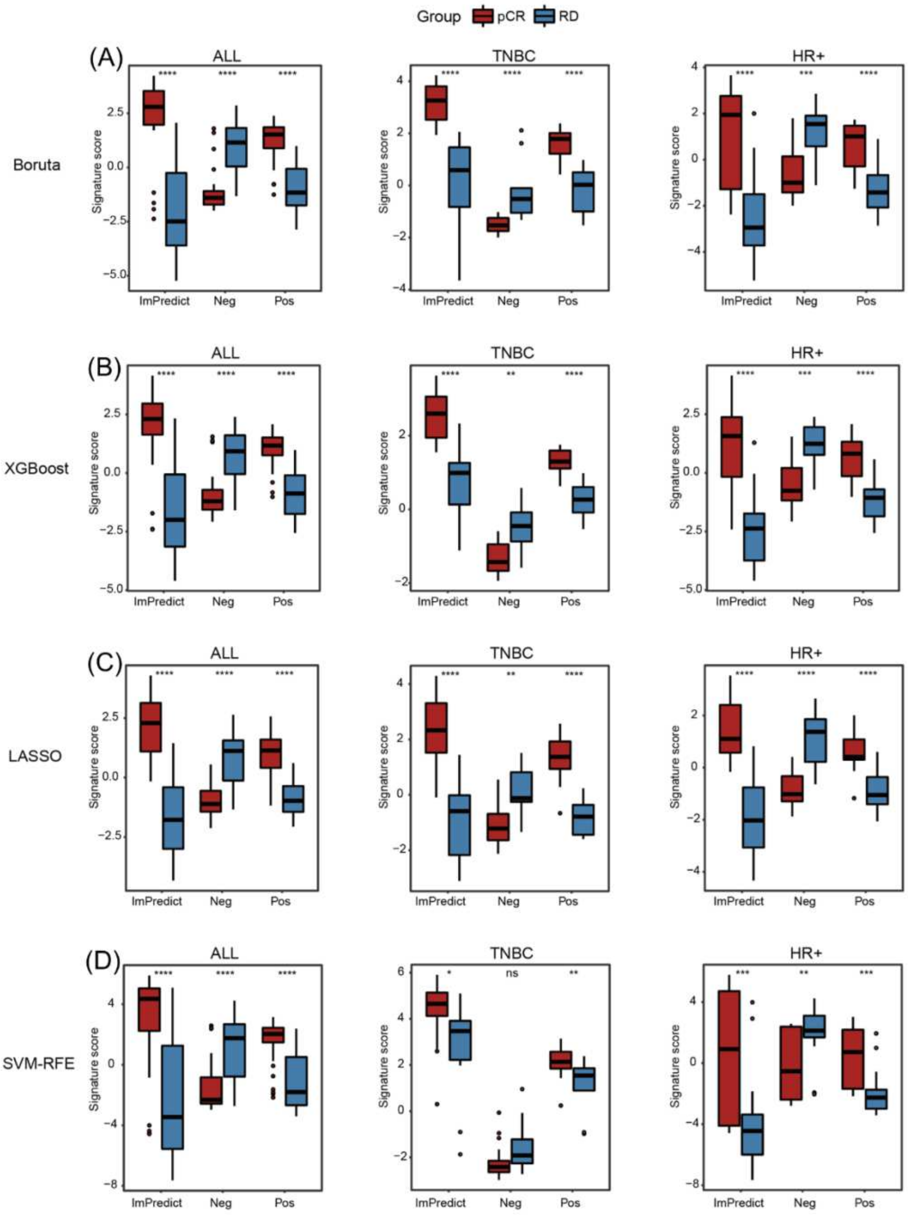

Figure S5. Distributions of the four signature scores derived from four algorithms in the pCR and RD groups of the discovery set.

(A) Boruta. (B) XGBoost. (C) LASSO. (D) SVM-RFE.

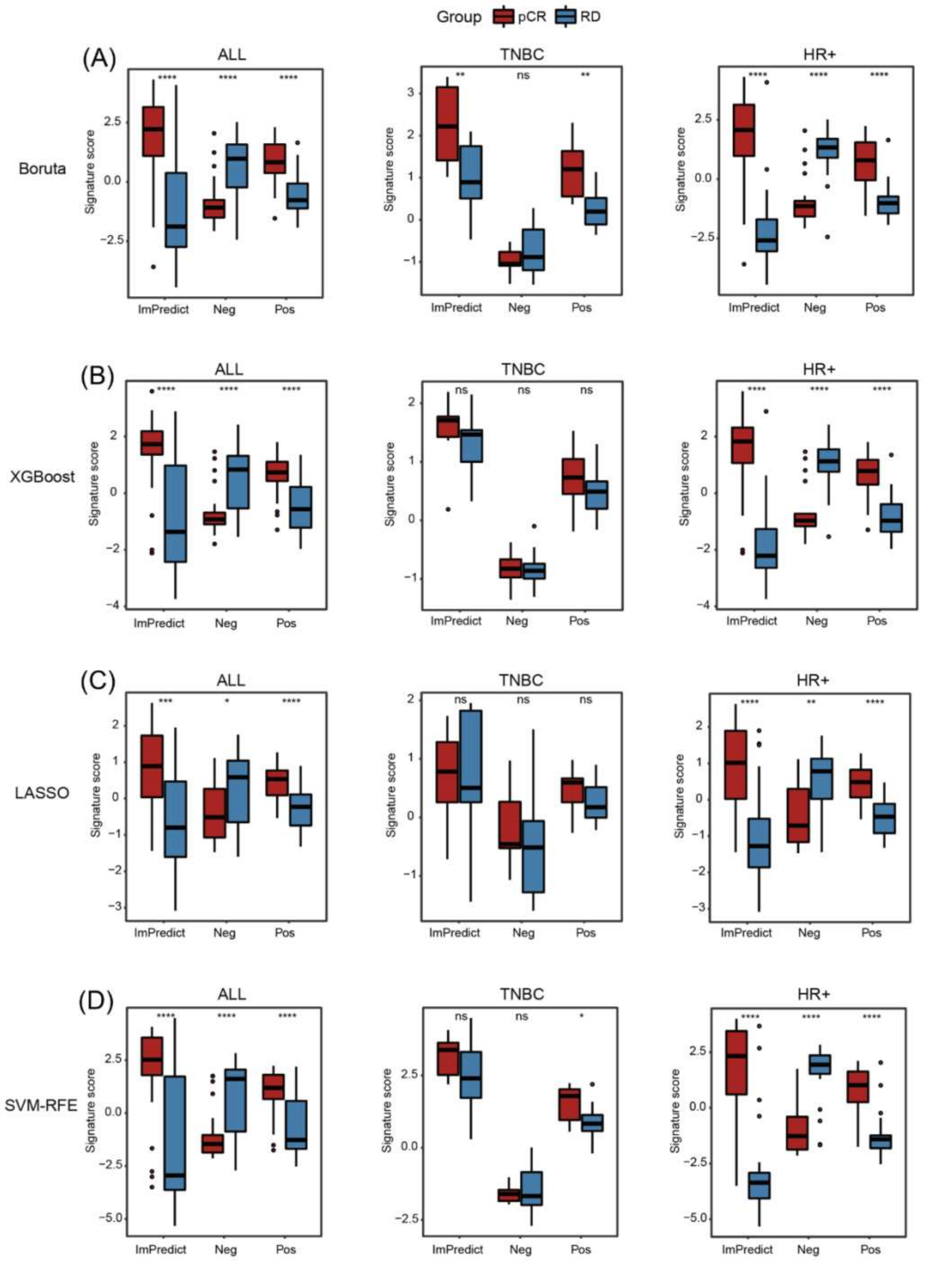

Figure S6. Distributions of the four signature scores derived from four algorithms in the pCR and RD groups of the validation set 1.

(A) Boruta. (B) XGBoost. (C) LASSO. (D) SVM-RFE.

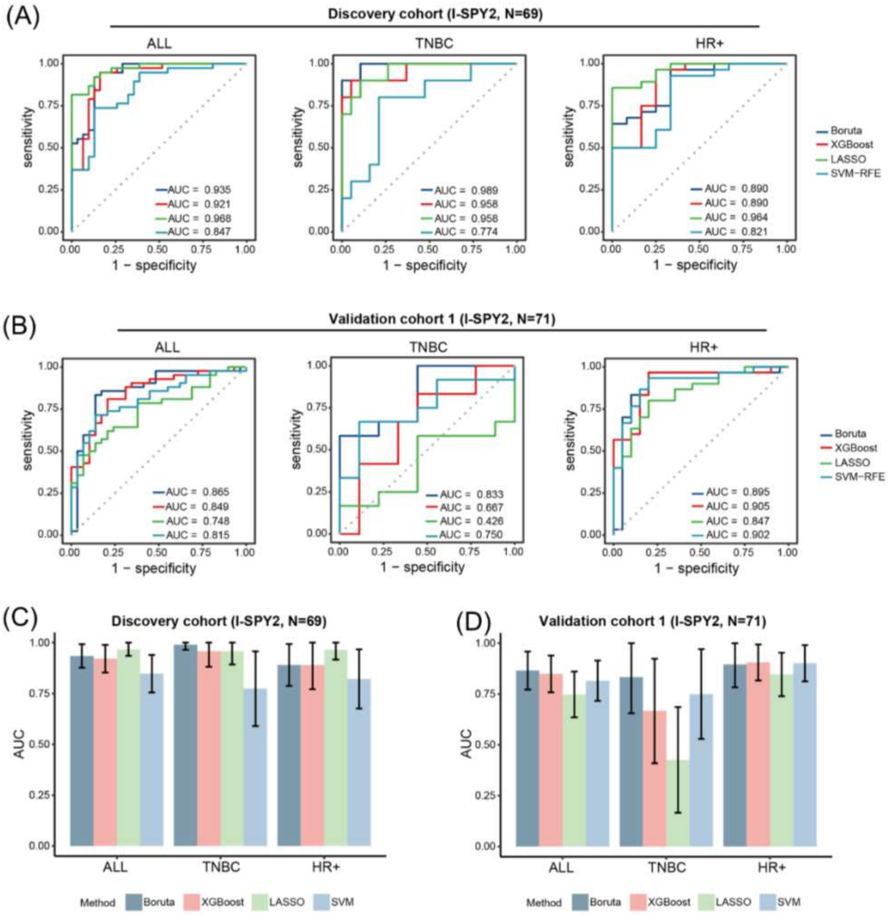

Figure S7. Predictive powers of the four signatures in the discovery set and validation set 1.

(A-B) ROC curves of the four signatures in the discovery set (A) and validation set 1 (B).

(C-D) AUCs of the four signatures in the discovery set (C) and validation set 1 (D).

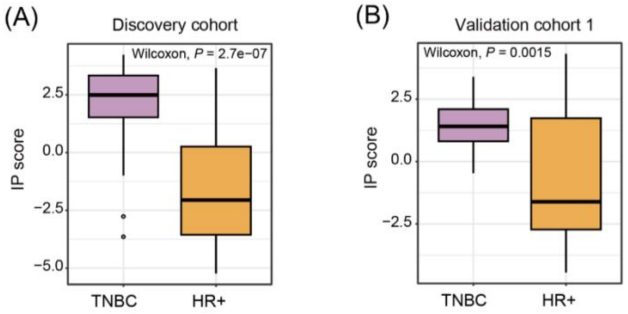

Figure S8. Distributions of the IP score between TNBC and HR+ BC in the discovery set and validation set 1.

(A) Discovery cohort. (B) Validation cohort 1.

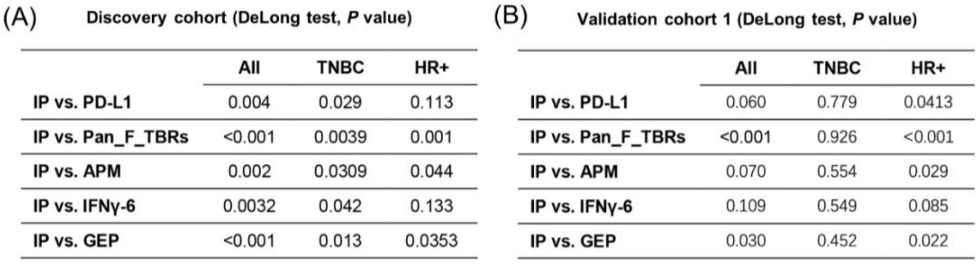

(A) **Discovery cohort (DeLong test, *P* value)**

	All	TNBC	HR+
IP vs. PD-L1	0.004	0.029	0.113
IP vs. Pan_F_TBRs	<0.001	0.0039	0.001
IP vs. APM	0.002	0.0309	0.044
IP vs. IFNγ-6	0.0032	0.042	0.133
IP vs. GEP	<0.001	0.013	0.0353

(B) **Validation cohort 1 (DeLong test, *P* value)**

	All	TNBC	HR+
IP vs. PD-L1	0.060	0.779	0.0413
IP vs. Pan_F_TBRs	<0.001	0.926	<0.001
IP vs. APM	0.070	0.554	0.029
IP vs. IFNγ-6	0.109	0.549	0.085
IP vs. GEP	0.030	0.452	0.022

Figure S9. DeLong tests of the IP score with five signatures in the discovery set and validation set 1. (A) Discovery cohort. (B) Validation cohort 1.

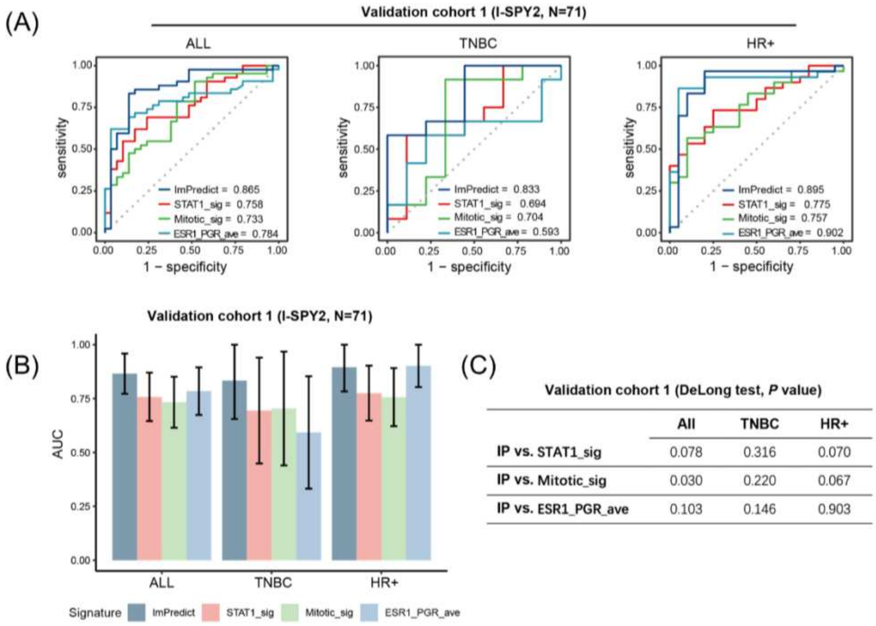

Validation cohort 1 (DeLong test, *P* value)

	All	TNBC	HR+
IP vs. STAT1_sig	0.078	0.316	0.070
IP vs. Mitotic_sig	0.030	0.220	0.067
IP vs. ESR1_PGR_ave	0.103	0.146	0.903

Figure S10. Comparison of the predictive effects of the IP score and feature signatures in the validation set 1.

(A) ROC curves of the IP score and feature signatures in the validation set 1.

(B) AUCs of the IP score and feature signatures in the validation set 1.

(C) DeLong tests of the IP score with three signatures in the validation set 1.

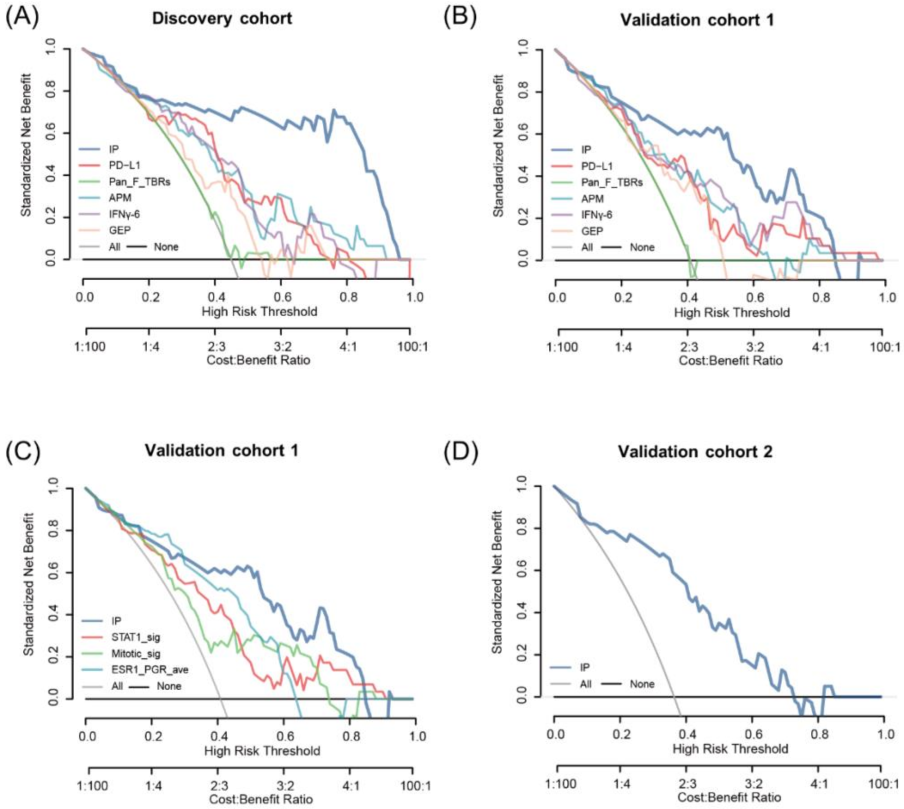

Figure S11. Predictive performances of the IP score and other signatures.

(A) DCA of the IP score and five predictive signatures in the discovery cohort.

(B) DCA of the IP score and five predictive signatures in the validation cohort 1.

(C) DCA of the IP score and three gene signatures in the validation cohort 1.

(D) DCA of the IP score in the validation cohort 2.

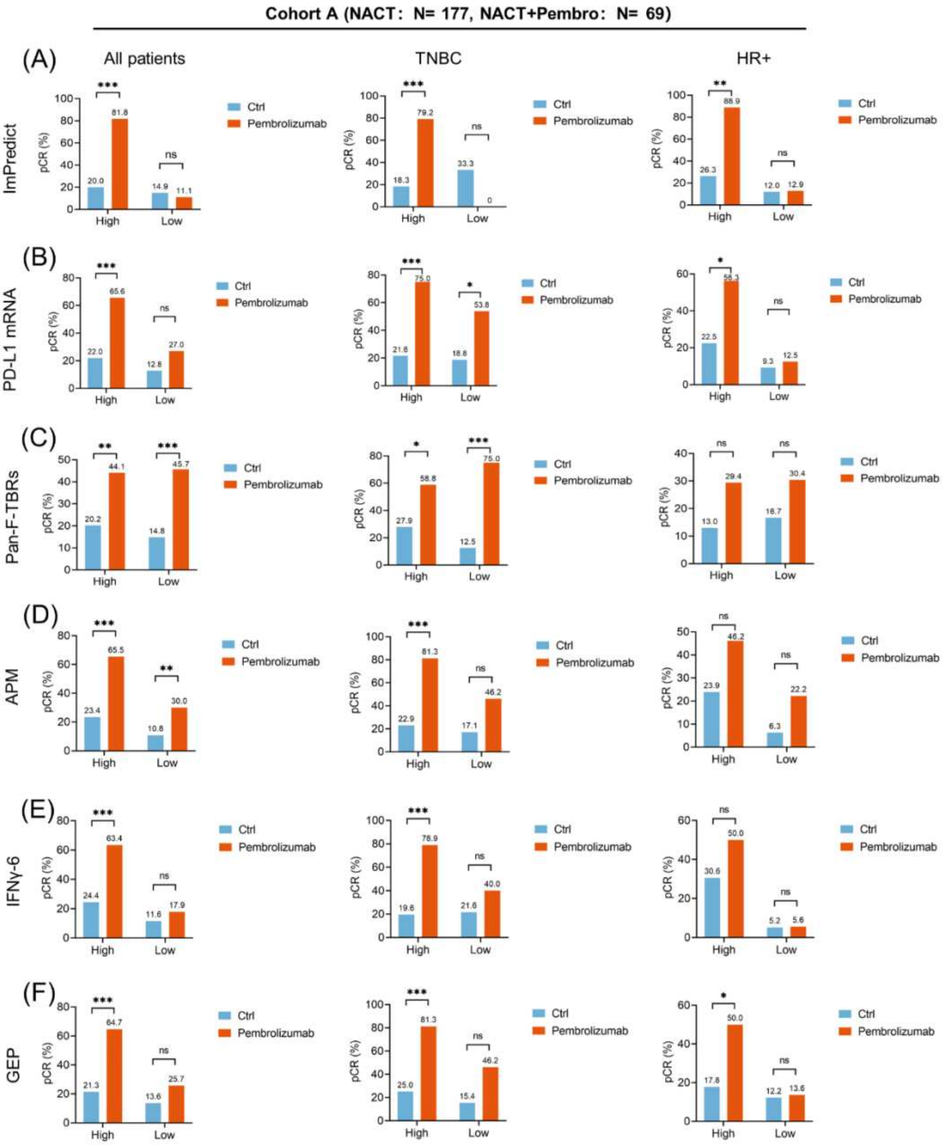

Figure S12. pCR rates in the high and low groups divided by the signature median in cohort A.

(A-F) pCR rates in the high and low groups divided by the signature medians of IP (A), PD-L1 mRNA (B), Pan-F-TBRs (C), APM (D), IFNγ-6 (E), and GEP (F), respectively.

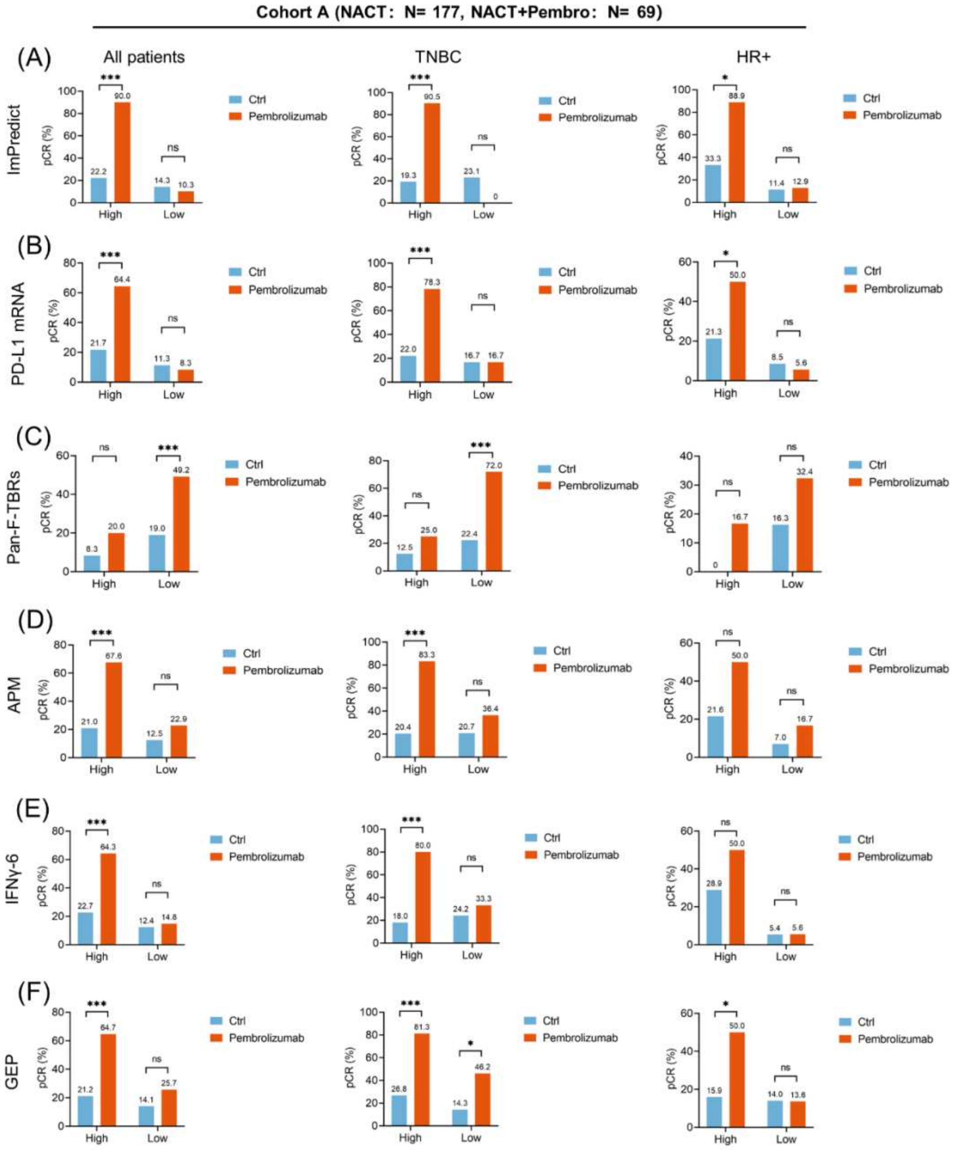

Figure S13. pCR rates in the high and low groups divided by the optimal cutoff in cohort A.

(A-F) pCR rates in the high and low groups divided by the optimal cutoff of predicting pCR in the immunotherapy arm of cohort A. IP (A), PD-L1 mRNA (B), Pan-F-TBRs (C), APM (D), IFNγ-6 (E), and GEP (F).

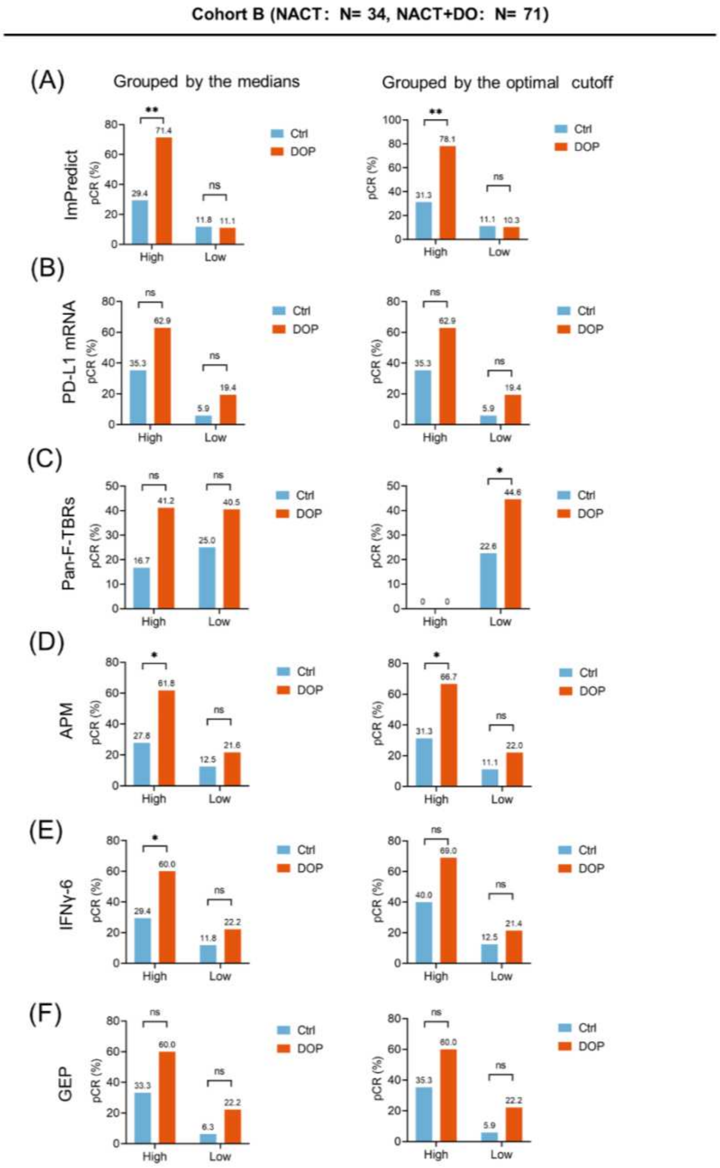

Figure S14. pCR rates in the high and low groups of cohort B.

(A-F) pCR rates in the high and low groups divided by the medians of signature scores or the optimal cutoffs of predicting pCR in the immunotherapy arm of cohort B. IP (A), PD-L1 mRNA (B), Pan-F-TBRs (C), APM (D), IFNγ-6 (E), and GEP (F).

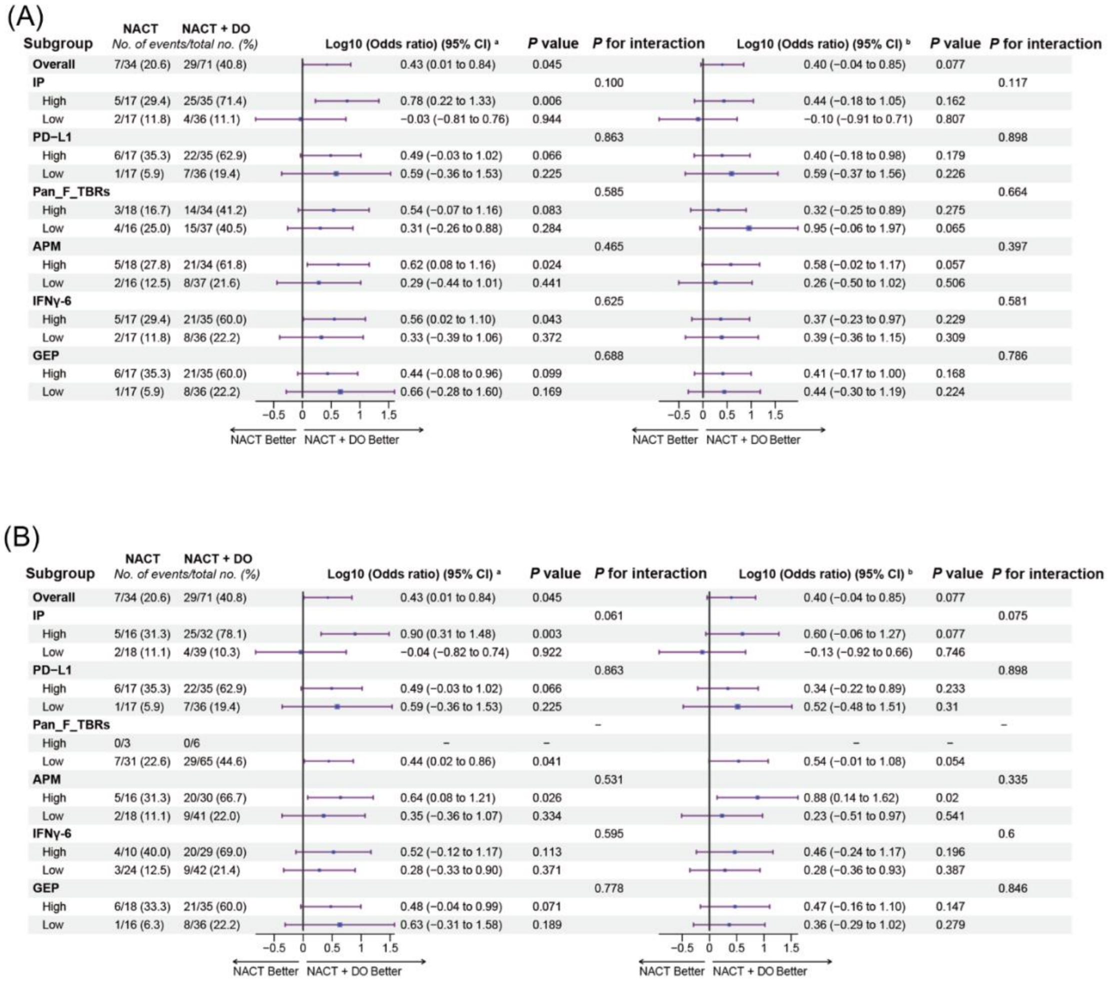

Figure S15. Marker-treatment interaction test in cohort B.

(A) Marker-treatment interaction test when the patients are grouped by the medians of signature scores in cohort B.

(B) Marker-treatment interaction test when the patients are grouped by optimal cutoff of predicting pCR in the immunotherapy arm of cohort B.

[a]indicates that the odds ratios are log10 transformed. [b]indicates that the odds ratios are HR-adjusted and log10 transformed.

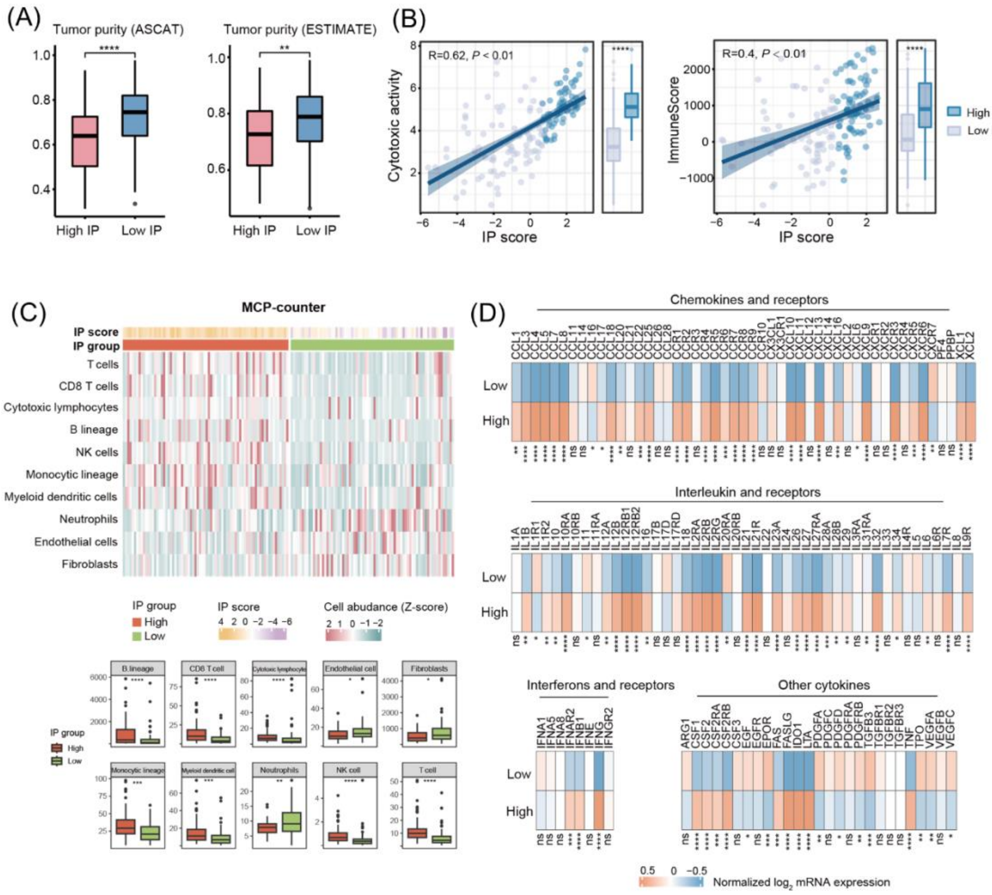

Figure S16. Landscape of the immune cells and cytokines in the high and low IP groups of the TCGA-TNBC cohort.

(A) Comparison of the tumor purity (left: ASCAT algorithm, right: ESTIMATE) in the high and low IP groups.

(B) Association of the IP score with CYT score and ImmuneScore.

(C) Heatmap and boxplots showing the microenvironment cell infiltrations in the high and low IP groups.

(D) Normalized mRNA expression levels of chemokines and receptors, interleukin and receptors, interferons and receptors, and other cytokines in the high and low IP groups.

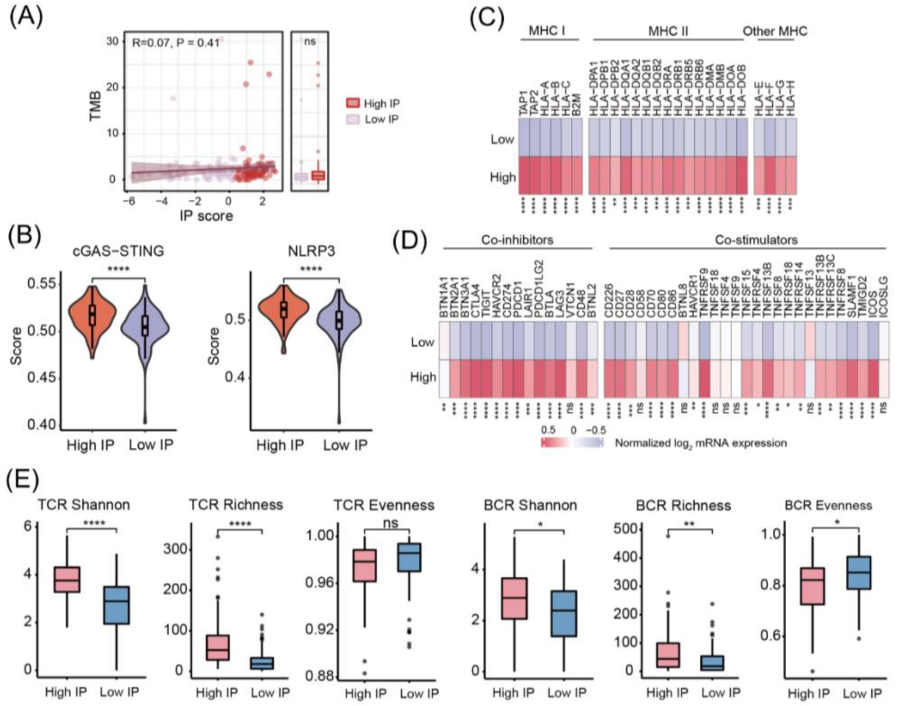

Figure S17. Differences in the immune response-related molecules and indicators between high and low IP groups of the TCGA-TNBC cohort.

(A) Relationship of the IP score with TMB.

(B) Comparison of two signature scores, cGAS-STING and the NLRP3 inflammasome, between the high and low IP groups.

(C-D) Normalized mRNA expression levels of MHC molecules (C), immune co-inhibitors and co-stimulators (D), in the high and low IP groups.

(E) Box plots showing the Shannon, Richness, and Evenness of TCR and BCR in the high and low IP groups.

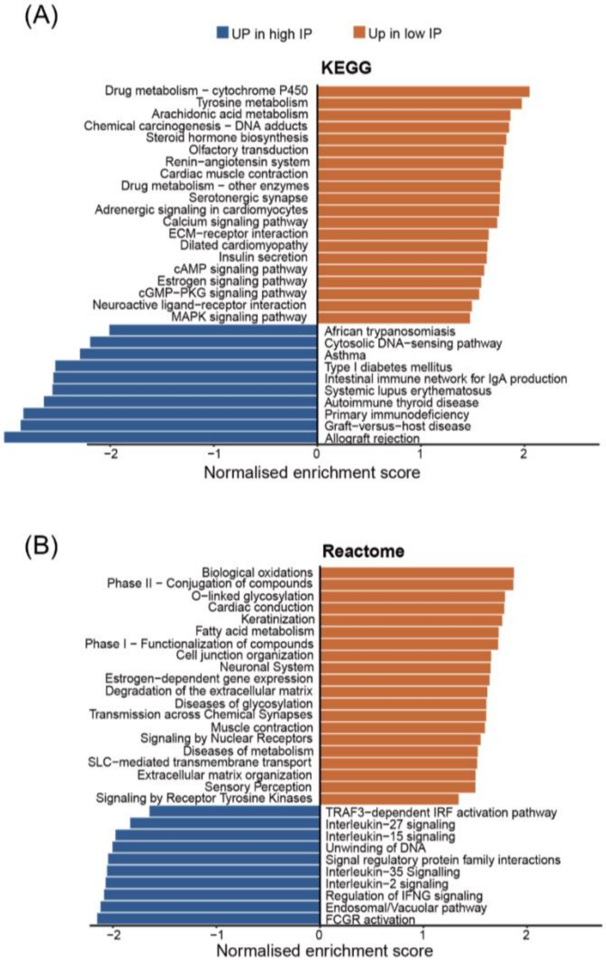

Figure S18. GSEA in the IP groups of the TCGA-TNBC cohort.
Different enriched KEGG (A) and Reactome (B) pathways in the high and low IP groups.

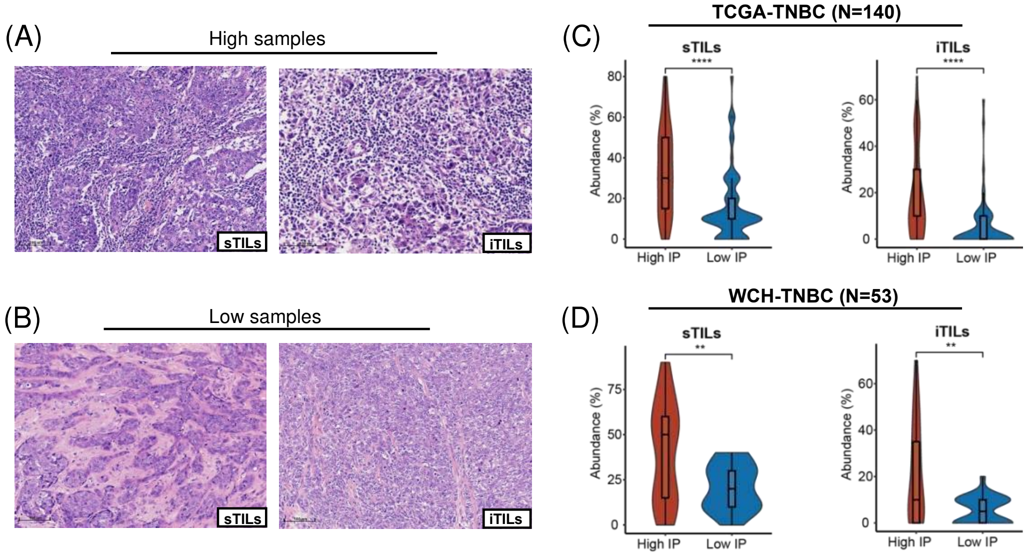

Figure S19. Pathologic scoring of sTILs and iTILs in the TCGA-TNBC and WCH-TNBC cohorts.

(A-B) Representative images of high TILs infiltration (A) and low TILs infiltration (B).

(C-D) Differences in the abundances of TILs in the high and low IP groups of the TCGA-TNBC (C) and WCH-TNBC (D) cohorts.

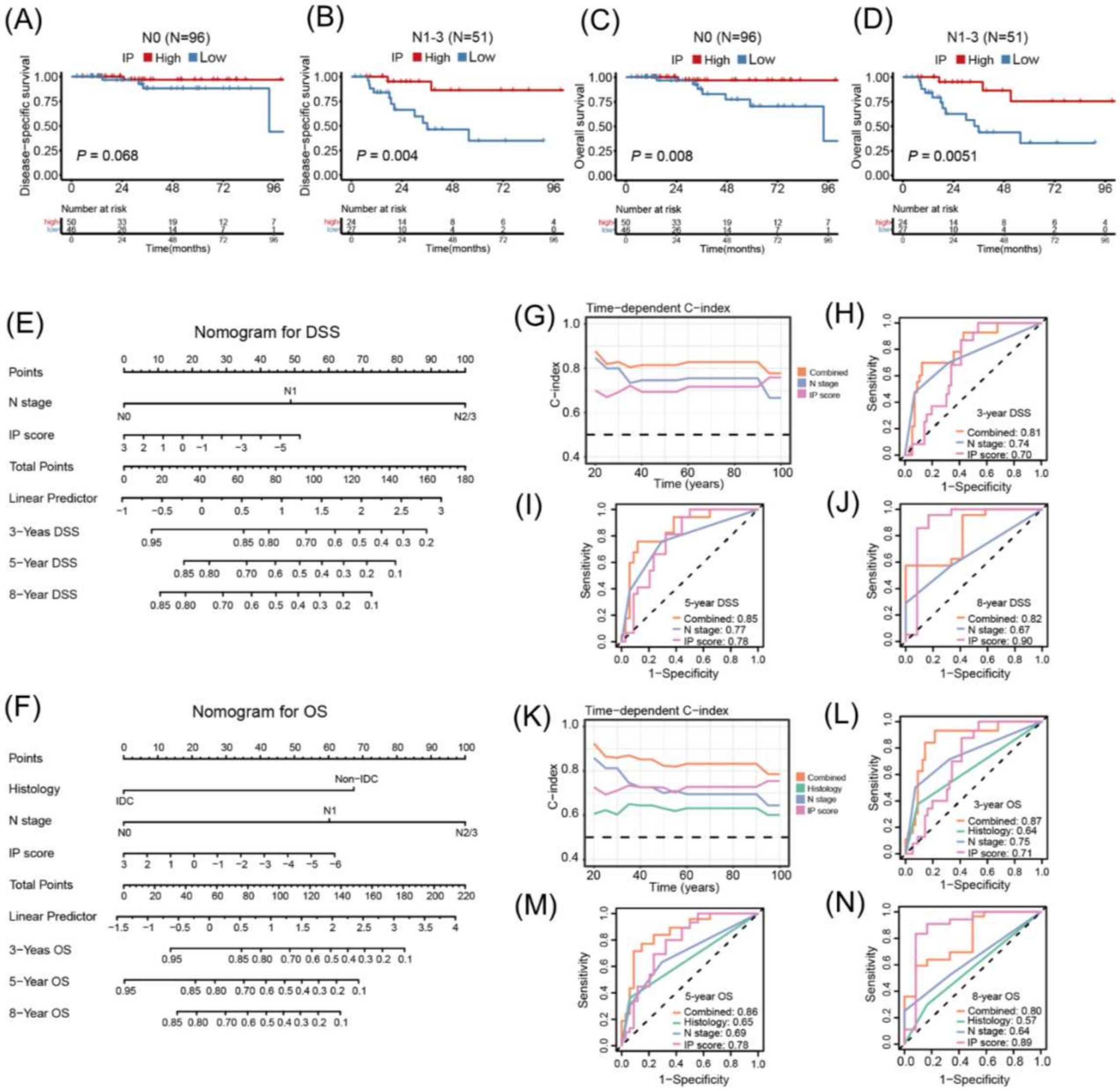

Figure S20. Evaluation of the prognostic significance of the IP score for TNBC.

(A-B) DSS of the high and low IP patients in the N0 (A) and N1-3 (B) groups.

(C-D) OS of the high and low IP patients in the N0 (C) and N1-3 (D) groups.

(E) Nomogram for predicting the probabilities of 3-, 5- and 8-year DSS.

(F) Nomogram for predicting the probabilities of 3-, 5- and 8-year OS.

(G) Time-dependent C-indices of the nomogram, N stage, and IP score for predicting DSS.

(H-J) ROC curves of the nomogram, N stage, and IP score concerning 3- (H), 5- (I), and 8-year (J) DSS.

(K) Time-dependent C-indices of the nomogram, histology, N stage, and IP score for predicting OS.

(L-M) ROC curves of the nomogram, N stage, and IP score concerning 3- (L), 5- (M), and 8-year (N) OS.